

Lepton flavor violating signals driven by CP symmetry of order 4

Bei Liu* and Igor P. Ivanov†

School of Physics and Astronomy, Sun Yat-sen University, 519082 Zhuhai, China

CP4 3HDM is a curious version of the three-Higgs-doublet model built upon a CP symmetry of order 4 (dubbed CP4). When extended to fermions, CP4 leads to unusually tight correlations between the scalar and Yukawa sectors and induces tree-level flavor changing neutral couplings. Still, viable scenarios exist, in which quark flavor changing signals remain within experimental limits. In this work, we extend CP4 to the lepton sector and investigate whether the lepton-Higgs couplings and lepton flavor violating (LFV) signals can also be kept under control. We consider two classes of LFV processes: tree-level lepton decays of the 125 GeV Higgs boson and one-loop radiative decay $\mu \rightarrow e\gamma$. For each CP4-invariant lepton Yukawa scenario, we perform a focused Yukawa sector scan that uses physical lepton properties as input and suppresses LFV effects. We identify a promising CP4 3HDM scenario compatible with the present-day experimental constraints, show that it can accommodate the recent CMS hint of a 146 GeV scalar decaying to $e\mu$, and argue that this interpretation can be tested at future colliders.

I. INTRODUCTION

Among many possible directions for building models beyond the Standard Model (BSM), multi-Higgs-doublet models remain a very popular framework that can offer remarkably rich BSM phenomenology with a minimum of assumptions. This research direction began half a century ago with T.D. Lee's construction of the two-Higgs-doublet model (2HDM) [1] and S. Weinberg's suggestion of the three-Higgs-doublet model [2]. Both models were proposed as possible explanations for the origin of *CP* violation. However, it was later recognized that such models offer interesting opportunities for flavor model building and can lead to characteristic collider signatures as well as peculiar cosmological consequences. As a result, the 2HDM and 3HDM literature now counts thousands of papers and continues to grow rapidly, see reviews [3, 4].

In the last decade, the exploration of 3HDMs picked up pace as they offer numerous opportunities that cannot be realized within the 2HDM or singlet extensions of the scalar sector. In particular, 3HDMs can be built upon various global symmetries, either exact or broken [5–9], which lead to characteristic signals worth exploring. When building such models, one usually tries to find a balance between the flexibility of the model and its predictive power. Models with a large symmetry content typically possess very few free parameters, are highly predictive, but conflict with experimental data. By relaxing symmetry assumptions, for example, by introducing soft breaking terms, one often succeeds in fitting experimental observations; however, with many additional free parameters, the model becomes less predictive and loses its theoretical appeal.

In [10], a peculiar version of the 3HDM was constructed, built on a single symmetry yet displaying a remarkably constrained scalar sector with unusual properties. The symmetry in question is a *CP* transformation of order 4, CP4 for short. Although higher-order *CP* transformations have been studied for decades [11–13], this was the first example of a multi-Higgs model, in which the imposition of CP4 did not lead to any accidental symmetry, as it happened, for instance, in the 2HDM [14–16]. Several phenomenological studies of the CP4 3HDM followed, focusing on the scalar sector [17, 18], the quark Yukawa sector [17, 19], or the Higgs-top-quark couplings [20, 21]. The main message that emerged from these studies is the following. Out of eight possible CP4-invariant quark scenarios, only one survives after the K , B , B_s , and D -meson oscillations as well as top-quark couplings are taken into account [21]. Admittedly, those works did not include all the experimental data available at present; thus, it remains an open question whether fully viable benchmark versions of the CP4 3HDM exist at all.

In this work, we explore for the first time whether extending CP4 to the lepton sector inevitably generates strong lepton-flavor-violating (LFV) signals that would be immediately ruled out by the present experimental constraints. It is well known that LFV processes are strongly suppressed in the SM and, therefore, are among the most sensitive probes of BSM physics, see review in [22–25]. Current experimental constraints on LFV are exceptionally tight. The MEG II experiment has set an upper limit of $\text{Br}(\mu \rightarrow e\gamma) < 1.5 \times 10^{-13}$ [26], and future experiments, such as Mu2e [27], will further tighten these constraints. The Particle Data Group lists strict bounds on various LFV decays of the SM-like Higgs boson [28], and one can expect these upper bounds to go down as the ATLAS and CMS

* liub98@mail2.sysu.edu.cn

† ivanov@mail.sysu.edu.cn

detectors accumulate more data. Thus, it is necessary to check whether any of the CP4-invariant lepton sectors with non-trivially transforming leptons have a chance of avoiding conflict with the existing data and which LFV signatures can be detected in future experiments.

In this work, we address these questions by extending CP4 to the lepton sector and performing a systematic phenomenological analysis of selected LFV signals. We explore the parameter space using the special scanning procedures developed previously for the scalar [18] and Yukawa [19] sectors of the model; these procedures use several physical observables as input, which strongly boosts the efficiency of the scan compared to the traditional approach of scanning the parameter space of the lagrangian. For each of the three CP4-invariant Yukawa cases, we calculate the tree-level lepton decays of h_{SM} , both flavor-conserving and flavor-violating, and one-loop radiative decay $\mu \rightarrow e\gamma$, which can be mediated by both neutral and charged Higgs bosons.

The outline of this paper is as follows. In section II, we review the scalar and lepton Yukawa sectors of the CP4 3HDM and list formulas used in numerical calculations. Section III presents numerical scans compared against experimental data. These results single out a specific CP4 3HDM lepton sector that passes all the constraints by a large margin. In section IV we show that the recent CMS hint at a leptonically decaying 146 GeV scalar can be accommodated and tested within this model. We finish by summarizing our results and provide auxiliary information in the appendices.

Throughout the paper, the fermion generations are labeled as i, j , while the three Higgs doublets are denoted with the subscripts a, b . When dealing with the five neutral Higgs bosons, we label them with $k = 1, \dots, 5$. With a slight abuse of notation, we use the same label k for the two charged Higgs bosons, with $k = 1, 2$. We believe that the choice is always clear and should not lead to confusion.

II. LFV PROCESSES IN THE CP4 3HDM

A. The scalar sector

For the completeness, we remind the reader of the basics of non-standard CP transformations and the CP4 symmetry.

In quantum field theory with several complex fields, the CP transformations is not defined uniquely [13, 29–31]. In a theory containing N complex scalar fields $\phi_a, a = 1, \dots, N$, one can define a general CP transformation (GCP) acting on the fields by $\phi_a \mapsto X_{ab}\phi_b^*$, with a unitary matrix X (the spatial coordinate inversion is implicitly assumed). Applying such a CP transformation twice, one generates a family transformation $\phi_a \mapsto (XX^*)_{ab}\phi_b$, which does not need to be the identity transformation. It can happen that the identity is reached only after imposing the CP transformation $2k$ times: $(XX^*)^k = \mathbb{I}$; in this case, we say the the CP transformation is of order $2k$. The usual CP is of order 2, and the first non-standard example of a CP transformation of order 4 (CP4 for short).

It is known that any CP4 transformation acting on three scalar fields can be represented, in a suitable basis, by the following transformation law [11–13]: $\phi_1 \mapsto \phi_1^*, \phi_2 \mapsto i\phi_3^*, \phi_3 \mapsto -i\phi_2^*$. The 3HDM scalar potential invariant under this transformation was constructed in [10] as a sum of two parts $V = V_0 + V_1$, where V_0 is invariant under all phase rotations of the doublets,

$$\begin{aligned} V_0 = & -m_{11}^2(\phi_1^\dagger\phi_1) - m_{22}^2(\phi_2^\dagger\phi_2 + \phi_3^\dagger\phi_3) + \lambda_1(\phi_1^\dagger\phi_1)^2 + \lambda_2 \left[(\phi_2^\dagger\phi_2)^2 + (\phi_3^\dagger\phi_3)^2 \right] \\ & + \lambda_{34}(\phi_1^\dagger\phi_1)(\phi_2^\dagger\phi_2 + \phi_3^\dagger\phi_3) - \lambda_4 \left[(\phi_1^\dagger\phi_1)(\phi_2^\dagger\phi_2) - (\phi_1^\dagger\phi_2)(\phi_2^\dagger\phi_1) + (\phi_1^\dagger\phi_1)(\phi_3^\dagger\phi_3) - (\phi_1^\dagger\phi_3)(\phi_3^\dagger\phi_1) \right] \\ & + \lambda'_{34}(\phi_2^\dagger\phi_2)(\phi_3^\dagger\phi_3) - \lambda'_4 \left[(\phi_2^\dagger\phi_2)(\phi_3^\dagger\phi_3) - (\phi_2^\dagger\phi_3)(\phi_3^\dagger\phi_2) \right], \end{aligned} \quad (1)$$

with all parameters real, while V_1 is given by

$$V_1 = \lambda_5(\phi_3^\dagger\phi_1)(\phi_2^\dagger\phi_1) + \lambda_8(\phi_2^\dagger\phi_3)^2 + \lambda_9(\phi_2^\dagger\phi_3)(\phi_2^\dagger\phi_2 - \phi_3^\dagger\phi_3) + h.c. \quad (2)$$

with a real λ_5 and complex λ_8, λ_9 . The notation used here follows the choice made in the most recent papers [18, 21]. We stress that the CP4 symmetry is exact; no soft breaking terms are introduced.

We assume that the parameters are such that minimum of potential is neutral and breaks CP4 symmetry. The latter requirement is needed because an unbroken global symmetry acting on scalars that participate in fermion mass generations will unavoidably lead to pathological quark sector [32]. The three initial Higgs doublets acquire vacuum expectation values (vevs) that may be complex. However, as shown in [17], after a suitable basis transformation that preserves the form of the potential, these vevs can be made real:

$$\langle \phi_a^0 \rangle = \frac{v}{\sqrt{2}}(c_\beta, s_\beta c_\psi, s_\beta s_\psi). \quad (3)$$

with $v = 246$ GeV and shorthand notation $c_x \equiv \cos(x)$, $s_x \equiv \sin(x)$. Thus, the position of the minimum is parameterized by two angles β and ψ .

Description of the scalar sector becomes more transparent if we pass from the original basis with the doublets ϕ_a to a Higgs basis with Φ_a , where only one doublet gets a non-zero vev: $\langle \Phi_1^0 \rangle = v/\sqrt{2}$, $\langle \Phi_2 \rangle = \langle \Phi_3 \rangle = 0$. Following the notation of [18, 19], we use the following transformation:

$$\begin{pmatrix} \Phi_1 \\ \Phi_2 \\ \Phi_3 \end{pmatrix} = \begin{pmatrix} c_\beta & s_\beta c_\psi & s_\beta s_\psi \\ -s_\beta & c_\beta c_\psi & c_\beta s_\psi \\ 0 & -s_\psi & c_\psi \end{pmatrix} \begin{pmatrix} \phi_1 \\ \phi_2 \\ \phi_3 \end{pmatrix}. \quad (4)$$

In this Higgs basis, we expand the doublets as

$$\Phi_1 = \frac{1}{\sqrt{2}} \begin{pmatrix} \sqrt{2}G_1^+ \\ v + \rho_1 + iG^0 \end{pmatrix}, \quad \Phi_2 = \frac{1}{\sqrt{2}} \begin{pmatrix} \sqrt{2}w_2^+ \\ \rho_2 + i\eta_2 \end{pmatrix}, \quad \Phi_3 = \frac{1}{\sqrt{2}} \begin{pmatrix} \sqrt{2}w_3^+ \\ \rho_3 + i\eta_3 \end{pmatrix}. \quad (5)$$

with G^0, G^\pm denoting the would-be Goldstone bosons. The five neutral and two charged fields can be organized as

$$\Psi_k = (\rho_1, \rho_2, \rho_3, \eta_3, \eta_2), \quad \Psi_k^\pm = (w_2^\pm, w_3^\pm). \quad (6)$$

We remind the reader that $k = 1, \dots, 5$ when labeling the neutral Higgs bosons and $k = 1, 2$ when denoting the charged Higgs bosons. The order of last two neutral components in Ψ_k (that is, η_3, η_2 , not η_2, η_3) is motivated by the tridiagonal form of the scalar mass matrix derived in [18]. These fields are not physical scalars, and both mass matrices (in the neutral and charged sectors) must be further diagonalized by appropriate rotations [18, 21].

In the exact scalar alignment, ρ_1 would be identical to the SM like Higgs boson $\rho_1 = h_{\text{SM}}$. However, the model does not force us to stick to the exact alignment. Following [18, 21], we allow for a small amount of misalignment. A convenient way to introduce it is to parametrize h_{SM} as

$$h_{\text{SM}} = \rho_1 c_\epsilon + s_\epsilon c_\alpha (c_{\gamma_1} \rho_2 + s_{\gamma_1} \rho_3) + s_\epsilon s_\alpha (c_{\gamma_2} \eta_3 + s_{\gamma_2} \eta_2), \quad (7)$$

where the four mixing angles $\epsilon, \alpha, \gamma_1, \gamma_2$ are taken as the input parameters in the scan of the scalar sector. This choice was instrumental for the so-called inversion algorithm developed in [18] for a much more efficient scalar space scanning procedure than the early study [17].

The key angle here is ϵ , which plays a role similar to $\beta - \alpha$ of the 2HDM, namely, it controls the coupling of h_{SM} to ZZ and WW pairs. The choice $\epsilon = 0$ would correspond to exact scalar alignment; but here, we consider a nonzero ϵ . It also affects the couplings of h_{SM} with the top quarks, both flavor-diagonal and flavor violating, such as $h_{\text{SM}} t \bar{u}$. The recent study [21] showed that values $|\epsilon| > 0.4$ can be disregarded as they almost always lead to a conflict with top-quark-related measurements.

All these relations allow us to choose the following parameters as input when scanning the scalar sector:

$$\{v, \beta, \psi, m_{\text{SM}}^2\}, \quad \{\epsilon, \alpha, \gamma_1, \gamma_2\}, \quad \{m_{H_1^\pm}^2, m_{H_2^\pm}^2, m_{11}^2 - m_{22}^2, \lambda_{89}\}, \quad (8)$$

where $\lambda_{89} = \sqrt{\text{Im}(\lambda_8)^2 + \text{Im}(\lambda_9)^2} > 0$, as [17, 18]. By performing our scalar scan in these parameters, we keep the properties of h_{SM} and charged Higgs bosons under tight control; all other scalar quantities such as λ_i or the properties of additional four neutral scalars can be numerically expressed through these input parameters.

B. The lepton Yukawa sector

CP4 symmetry was extended to the quark Yukawa sector in [10, 19], where the very specific forms of the quark Yukawa matrices were derived. These findings are equally applicable to the lepton Yukawa sector. If needed, right-handed neutrinos can also be introduced in this model, as was done in [33]; however, since our focus here is on the charged lepton signals, we do not introduce them in this work. To set up the notation, we write the lepton Yukawa sector in any 3HDM is given by

$$-\mathcal{L}_Y = \bar{L}_L^0 (\Gamma_1 \phi_1 + \Gamma_2 \phi_2 + \Gamma_3 \phi_3) e_R^0 + h.c. \quad (9)$$

The lepton generation indices are implicitly assumed. The superscript 0 refers to the fact that these fields are the starting lepton fields before mass matrix diagonalization; we will remove the superscript when we pass to the physical leptons. When required to be invariant under CP4, the lepton Yukawa matrices $\Gamma_a, a = 1, 2, 3$ can only assume very special textures labeled in [17] as cases A, B_1, B_2, B_3 .

It must be said that case *A* corresponds to the trivial scenario of all leptons coupling only to the first Higgs doublet. As a result, all lepton fields transform trivially under CP4, and LFV signals are absent. This possibility is certainly available within CP4 3HDM and was implicitly assumed in the previous works. What we explore in this paper is whether any *non-trivial* CP4 scenario, B_1 , B_2 , or B_3 —with all Γ_a unavoidably non-zero in each of these cases—can also be made compatible with the present LFV experimental constraints.

Upon electroweak symmetry breaking, the mass matrix of charged leptons in the real vevs basis of Eq. (3) is

$$M_e^0 = \frac{v}{\sqrt{2}} (\Gamma_1 c_\beta + \Gamma_2 s_\beta c_\psi + \Gamma_3 s_\beta s_\psi). \quad (10)$$

In general, this mass matrix is non-diagonal and complex, and can be diagonalized by the following three-dimensional unitary transformations of the lepton fields $e_L^0 = V_L e_L$, $e_R^0 = V_R e_R$, $\nu_L^0 = U_L \nu_L$. These transformations lead to the Pontecorvo-Maki-Nakagawa-Sakata (PMNS) matrix: $V_{\text{PMNS}} = U_L^\dagger V_L$, or $U_L = V_L V_{\text{PMNS}}^\dagger$. The interaction of the neutral (complex) components of the scalar doublets with the leptons can be described in the Higgs basis as

$$\Gamma_1 \phi_1 + \Gamma_2 \phi_2 + \Gamma_3 \phi_3 = \frac{\sqrt{2}}{v} (\Phi_1 M_e^0 + \Phi_2 N_2^0 + \Phi_3 N_3^0), \quad (11)$$

where

$$N_2^0 = \frac{v}{\sqrt{2}} (-\Gamma_2 s_\psi + \Gamma_3 c_\psi), \quad N_3^0 = \frac{v}{\sqrt{2} s_\beta} \Gamma_1 - M_d^0 \cot \beta = M_d^0 \tan \beta - \frac{v}{\sqrt{2} c_\beta} (\Gamma_2 c_\psi + \Gamma_3 s_\psi). \quad (12)$$

After the rotation of lepton fields, we get $V_L^\dagger M_e^0 V_R = \text{diag}(m_e, m_\mu, m_\tau) \equiv M_e$, $V_L^\dagger N_{2,3}^0 V_R = N_{2,3}$, and consequently, $U_L^\dagger N_{2,3}^0 V_R = V_{\text{PMNS}} N_{2,3}$. The Yukawa matrices N_2 , N_3 describe the couplings across the lepton generations of the complex fields present in Φ_2 and Φ_3 , both neutral and charged. As for PMNS matrix parameters, we adopt the standard PDG values [28, 34–36]:

$$\theta_{12} = 33.6^\circ, \quad \theta_{23} = 46.9^\circ, \quad \theta_{13} = 8.5^\circ. \quad (13)$$

As for the leptonic *CP*-violating phase, we choose $\delta = 210^\circ$ [37]. Its experimental value still bears large uncertainties but it does not have any noticeable impact on our results; this was verified by comparing the scatter plots presented below for the values of $\delta = 0, \pi, 3\pi/2$.

When performing a scan in the lepton Yukawa sector, we adapt the inversion procedure developed in [19] for the quark sector. We take the physical lepton masses and the PMNS matrix as input, parametrize V_L, V_R appropriately, and express N_2, N_3 in terms of these parameters. Explicit expressions for N_2, N_3 in cases B_1, B_2, B_3 are provided in Appendix A. It is worth pointing out that these coupling matrices are independent of the scalar sector angle ψ .

C. Physical Higgs-lepton couplings

In the Higgs basis of Eq. (5), the scalar sector contains five real and two complex scalar fields, apart from the would-be Goldstone bosons. Their couplings to the physical leptons are described by

$$-\mathcal{L}_Y = \frac{1}{v} \bar{e}_{Li} [(M_e)_{ij} \rho_1 + (N_2)_{ij} (\rho_2 + i\eta_2) + (N_3)_{ij} (\rho_3 + i\eta_3)] e_{Rj} + h.c. \quad (14)$$

$$-\mathcal{L}'_Y = \frac{\sqrt{2}}{v} \bar{\nu}_{Li} [(V_{\text{PMNS}} N_2)_{ij} w_2^+ + (V_{\text{PMNS}} N_3)_{ij} w_3^+] e_{Rj} + h.c. \quad (15)$$

The physical neutral Higgs bosons H_k , with $k = 1, \dots, 5$, are linear combinations of the five neutral scalar fields, with their mixing described by a 5×5 rotation matrix. Similarly, physical charged Higgs bosons H_k^\pm , $k = 1, 2$, arise from mixing of w_2^\pm and w_3^\pm . All these expressions can be computed numerically for any point of the scan.

We parameterize the Yukawa interaction between physical leptons and physical scalars via their coupling matrices Y^k (neutral Higgs bosons) and Z^k (charged Higgs bosons):

$$-\mathcal{L}_Y = \bar{e}_{Li} Y_{ij}^k H_k e_{Rj} + \bar{\nu}_{Li} (Y^{k\dagger})_{ij} H_k \nu_{Lj}. \quad (16)$$

$$-\mathcal{L}'_Y = \bar{\nu}_{Li} Z_{ij}^k H_k^+ e_{Rj} + \bar{e}_{Li} (Z^{k\dagger})_{ij} H_k^- \nu_{Lj}. \quad (17)$$

For the SM-like Higgs boson h_{SM} , the coupling matrix, which we denote simply as Y_{ij} , can be written in terms of the familiar angles $\epsilon, \alpha, \gamma_1, \gamma_2$ defined in Eq. (7):

$$Y_{ij} = c_\epsilon \cdot \frac{m_i}{v} \delta_{ij} + s_\epsilon \cdot \left[\frac{(N_2)_{ij}}{v} (c_\alpha c_{\gamma_1} + i s_\alpha s_{\gamma_1}) + \frac{(N_3)_{ij}}{v} (c_\alpha s_{\gamma_1} + i s_\alpha c_{\gamma_1}) \right]. \quad (18)$$

The matrices N_2 and N_3 both modify the diagonal entries and generate nonzero off-diagonal entries leading to LFV decays of the 125 GeV Higgs boson.

Each additional neutral Higgs boson H_k can be expanded in the basis of $\Psi_{k'} \equiv (\rho_1, \rho_2, \eta_2, \rho_3, \eta_3)$ as $H_k = c_{k'}^k \Psi_{k'}$, where $c_{k'}^k$ are just the entries of the unitary 5×5 diagonalizing matrix. Then, the coupling matrix Y^k is

$$Y_{ij}^k = c_1^k \cdot \frac{m_i}{v} \delta_{ij} + \frac{(N_2)_{ij}}{v} (c_2^k + i c_3^k) + \frac{(N_3)_{ij}}{v} (c_4^k + i c_5^k). \quad (19)$$

Finally, for the charged Higgs bosons $H_k^\pm = e_k^\pm w_{k'}^\pm$, their coupling matrices Z_{ij}^k are similarly written as

$$Z_{ij}^k = \frac{\sqrt{2}}{v} [(V_{\text{PMNS}} N_2)_{ij} \cdot e_1^k + (V_{\text{PMNS}} N_3)_{ij} \cdot e_2^k]. \quad (20)$$

With this parametrization, and adopting the ultrarelativistic approximation for the produced leptons, the decay widths of any Higgs boson to two leptons can be written as

$$\Gamma(H_k \rightarrow \ell_i^\mp \ell_j^\pm) = \frac{m_{H_k}}{8\pi} (|Y_{ij}^k|^2 + |Y_{ji}^k|^2), \quad \Gamma(H_k \rightarrow \ell_i^- \ell_i^+) = \frac{m_{H_k}}{8\pi} |Y_{ii}^k|^2. \quad (21)$$

A key goal of this work is to identify the parameter regions where these Higgs-lepton couplings comply with experimental constraints on h_{SM} lepton decays.

D. Muon radiative decay: $\mu \rightarrow e\gamma$ at one loop

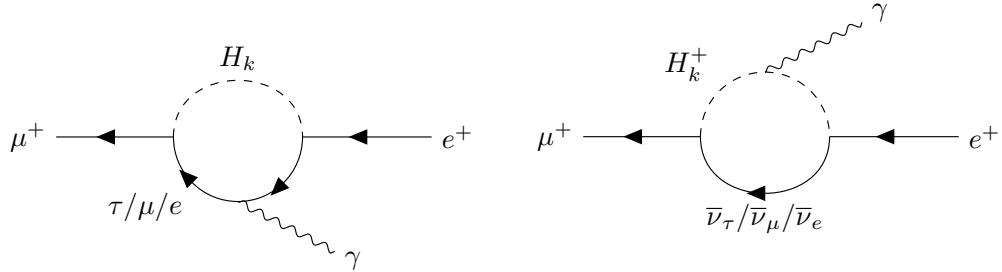


Figure 1. One-loop Feynman diagrams for $\mu^+ \rightarrow e^+ \gamma$ due to neutral Higgs bosons (left) and charged Higgs bosons (right).

Another critical test of a non-trivially transforming leptonic sector of the CP4 3HDM is the radiative LFV decay $\mu \rightarrow e\gamma$. In NHDM, contributions to this decay start from one-loop diagrams shown in Fig. 1. It has been pointed out [38–40] that the two-loop diagrams could also give a sizable contribution if a large hierarchy between the various Yukawa couplings takes place. Although it may indeed be the case in the CP4 3HDM, we do not think such a laborious computation is needed in our case. Indeed, our goal is not to give a precise prediction for such decays within specific benchmark points but to understand whether such decays could be suppressed at all below the presently reported experimental bound. Besides, two-loop contributions unavoidably involve the CP4 3HDM quark sector, which goes beyond our task. Thus, we find it sufficient to limit our analysis only to the one-loop contributions.

For the one-loop result of the branching ratio $\mathcal{B}_{e\gamma}^\mu$, we adopt the expressions given in [41]:

$$\text{Br}(\mu \rightarrow e\gamma) \equiv \mathcal{B}_{e\gamma}^\mu = \frac{m_\mu^5}{4\pi\Gamma_\mu} (|c_R^{e\mu}|^2 + |c_L^{e\mu}|^2). \quad (22)$$

The Wilson coefficients c_R and c_L receive contributions from both diagrams in Fig. 1: $c_R^{e\mu} = (c_R^{e\mu})_{n.} + (c_R^{e\mu})_{ch.}$ and $c_L^{e\mu} = (c_L^{e\mu})_{n.} + (c_L^{e\mu})_{ch..}$ All neutral Higgs bosons H_k give the following contribution to $c_R^{e\mu}$:

$$(c_R^{e\mu})_{n.} = \sum_{k=1}^5 \sum_{j=e,\mu,\tau} \frac{-e}{96\pi^2 m_{H_k}^2} \left[Y_{ej}^k Y_{\mu j}^{k*} + \frac{m_e}{m_\mu} Y_{je}^{k*} Y_{j\mu}^k - \frac{m_j}{m_\mu} Y_{ej}^k Y_{j\mu}^k (9 - 6 \ln \frac{m_{H_k}^2}{m_j^2}) \right]. \quad (23)$$

The total neutral Higgs boson contribution $(c_L^{e\mu})_{n.}$ can be obtained from Eq. (23) by exchanging Y_{ij} with Y_{ji}^* . The total contribution of the two charged Higgs bosons $c_R^{e\mu}$ and $c_L^{e\mu}$ are given by

$$(c_R^{e\mu})_{ch.} = \sum_{k=1}^2 \sum_{j=\nu_e,\nu_\mu,\nu_\tau} \frac{e}{192\pi^2 m_{H_k^\pm}^2} Z_{j\mu}^k Z_{je}^{k*}, \quad (c_L^{e\mu})_{ch.} = \frac{m_e}{m_\mu} (c_L^{e\mu})_{ch..} \quad (24)$$

III. NUMERICAL RESULTS

A. The scan procedure and constraints

With the expressions for the leptonic decays of h_{SM} and for the branching ratio of $\mu \rightarrow e\gamma$, we are now ready to perform a numerical scan in the CP4 3HDM parameter space and explore the constraints on the model arising from the experimental data. In this section, we present the results of this study, using as the key example the CP4-invariant lepton sector B_1 . As we will see below, this is the most promising scenario, as its parameter space includes regions that satisfy all the experimental bounds by a large margin. The two other cases, B_2 and B_3 , can be treated in a similar way and typically lead to stronger LFV signals; their results are reported at the end of this section.

Our scan procedure consists of two steps. First, we scan the scalar sector and filter out a substantial sample of scalar parameter space points that satisfy all the theoretical constraints; then, this sample is used as input for the lepton sector scan. It is known that a generic scan in the scalar sector of the CP4 3HDM typically produces one or several Higgs bosons lighter than the top quark [17]. Although such situations are not ruled out [21], we prefer to focus on the region with all non-standard scalars as heavy as possible. To this end, we follow the procedure developed in [18] and perform a restricted scan in the scalar sector that highlights the high-mass region. This is done with the following ranges of the input parameters:

$$\begin{aligned} \tan \beta &\in [0.5, 2], \quad \tan \psi \in [0.5, 3], \quad |\epsilon| < 0.3, \quad |\tan \alpha| < 0.05, \quad |\tan \gamma_1|, |\tan \gamma_2| < 0.3, \\ m_{11}^2 - m_{22}^2 &\in [-(300 \text{ GeV})^2, (300 \text{ GeV})^2], \quad m_{H_k^\pm}^2 \in [0, (700 \text{ GeV})^2], \quad \lambda_{89} \in (0, 4). \end{aligned} \quad (25)$$

Then we reconstruct numerically all the parameters of the potential and impose the standard theoretical constraints: the bounded-from-below (BFB) conditions [10]; the unitarity and perturbativity constraints following the simplified approach of [17] (although it must be mentioned that the exact conditions are now known [42]); the electroweak precision parameters S, T , and U , which are required to lie within the 2σ ranges of their experimental values [43]. We then compute the scalar mass matrices, diagonalize them numerically, and obtain the masses of all other Higgs bosons, as well as the entries of the diagonalizing matrices $c_{k'}^k$ and $e_{k'}^k$, and select only the points for which all additional neutral Higgs bosons are heavier than h_{SM} .

As for the leptonic sector scan, we adopt the inversion procedure developed in [19] for the lepton sector, using the scalar sector sample as input, along with the angles of the rotation matrices V_L, V_R, U_L , which are constrained by the PMNS matrix. In the initial scan, we allow these angles to vary over their entire domains. However, we will later switch to a restricted scan where the relevant angles are sampled in a tightly constrained interval to further suppress LFV signals.

For the experimental limits on the LFV decay branching ratio of h_{SM} , we use the 95%CL limits listed by the Particle Data Group (PDG) [28], which are based on the experimental results reported in [44–46]:

$$\text{Br}(h_{\text{SM}} \rightarrow e\mu) < 4.4 \times 10^{-5}, \quad \text{Br}(h_{\text{SM}} \rightarrow e\tau) < 2.0 \times 10^{-3}, \quad \text{Br}(h_{\text{SM}} \rightarrow \mu\tau) < 1.5 \times 10^{-3}. \quad (26)$$

For the lepton flavor-conserving (LFC) decay modes, we use the experimental results from [47–50] compiled by PDG:

	SM, Ref. [51]	PDG	(27)
$\text{Br}(h_{\text{SM}} \rightarrow ee)$	5×10^{-9}	$< 3.0 \times 10^{-4}$	
$\text{Br}(h_{\text{SM}} \rightarrow \mu\mu)$	2.15×10^{-4}	$\mu_{\mu\mu}^h = 1.4 \pm 0.4$	
$\text{Br}(h_{\text{SM}} \rightarrow \tau\tau)$	6.2×10^{-2}	$\mu_{\tau\tau}^h = 0.97 \pm 0.11$	

Here, $\mu_{\ell\ell}^h = \text{Br}(h_{\text{SM}} \rightarrow \ell\ell)/[\text{Br}(h_{\text{SM}} \rightarrow \ell\ell)]_{\text{SM}}$ are the usual signal strengths of the leptonic decays channels.

Finally, the experimental upper limit is $\text{Br}(\mu \rightarrow e\gamma) < 1.5 \times 10^{-13}$, [26].

B. Case B_1 : leptonic decays of h_{SM}

Before presenting the results of the full scan, let us explore how the leptonic decays of h_{SM} depend on the parameters. As can be seen from Eq. (18), the key role is played by the misalignment angle ϵ : the closer this angle to zero, the weaker are the departures from the SM predictions, both in the LFC and LFV decays. For small ϵ , the branching ratios of the LFC and LFV decays deviate from their SM values by s_ϵ and s_ϵ^2 , respectively. The patterns of these departures, which come from the matrices N_2 and N_3 , significantly depend on $\tan \beta$ but not on ψ .

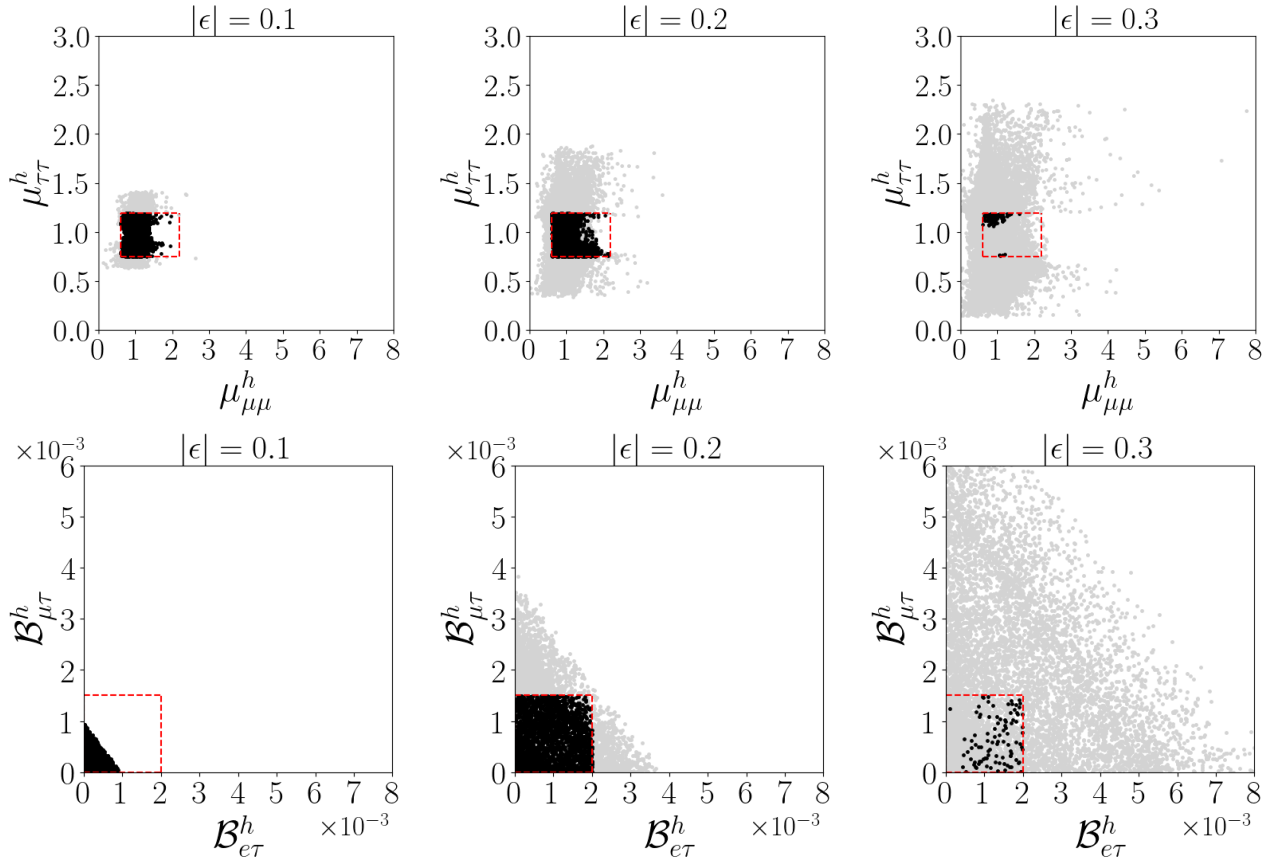


Figure 2. The impact of the misalignment angle ϵ on the LFC (top row) and LFV (bottom row) decays of h_{SM} . The dashed red box shows the experimental limits. The points which satisfy all six experimental limits are shown as black dots.

In Fig. 2, we show the impact of ϵ on the LFC (top row) and LFV (bottom row) decays of h_{SM} . In these plots, we use the shorthand notation $\mathcal{B}_{\ell_i \ell_j}^h \equiv \text{Br}(h_{\text{SM}} \rightarrow \ell_i \ell_j)$. When a generated point satisfies all six experimental limits, we plot it as a black dot; if at least one constraint is violated, it is plotted in gray. The red dashed boxes indicate the experimental constraints within each plane. As $|\epsilon|$ increases, the departures from the SM predictions grow as expected. For $|\epsilon| \leq 0.1$, most sampled points are still within the experimental limits. For $|\epsilon| > 0.3$, very few randomly selected points fall within the experimental limits, the strongest constraints coming from $h_{\text{SM}} \rightarrow \tau\tau$ and the LFV decays. In addition, it was shown in [21] that the couplings $h_{\text{SM}} t\bar{t}$ and $h_{\text{SM}} u\bar{u}$ become strong and violate experimental constraints on the Higgs-top processes. With these results, we focus on the region $|\epsilon| \leq 0.3$ in the subsequent analysis. Note that these constraints are stronger than those coming from the $h_{\text{SM}} VV$ couplings [21].

Another important parameter, $\tan \beta$, influences the patterns of the Yukawa matrices N_2 and N_3 . Ref. [19] contains explicit expression for N_2, N_3 for up and down quarks. One leptonic sector matrices repeat their expressions for the down-quark sector and are collected in Appendix A. For the Yukawa sector B_1 , which our main scenario here, the matrix N_2 has the form

$$N_2 = V_L^\dagger R_3^0 V_L \cdot M_d, \quad \text{where} \quad R_3^0 = \text{diag}(\cot \beta, \cot \beta, -\tan \beta). \quad (28)$$

It is clear from this expression that the magnitude of the LFV elements is controlled by the rotation angles of the left-handed charged lepton diagonalizing matrix V_L , while its diagonal elements are controlled by $\tan \beta$. As for N_3 , its main dependence on β comes from the $1/\sin \beta$ prefactor, see Appendix A. However, the physical Higgs bosons receive contributions from both N_2 and N_3 , which results in a non-trivial interplay of the two structures.

Fig. 3 shows the LFC and LFV decays for $\tan \beta = 0.5, 1$, and 2 ; the other parameters are scanned over. Both LFV decay contours/density and LFC decay contours exhibit strong correlation with $\tan \beta$. Overall, within the selected scanning range of $\tan \beta$, a significant fraction of random scan points satisfy all the six experimental constraints.

With these insights in mind, we can combine the scalar sector scan within the high-mass range Eq. (25) with the leptonic Yukawa sector and explore the leptonic decays of h_{SM} . These results are summarized in Fig. 4. The difference with respect to the previous plots is that we now do not slice the parameter space at fixed ϵ or fixed $\tan \beta$ but scan

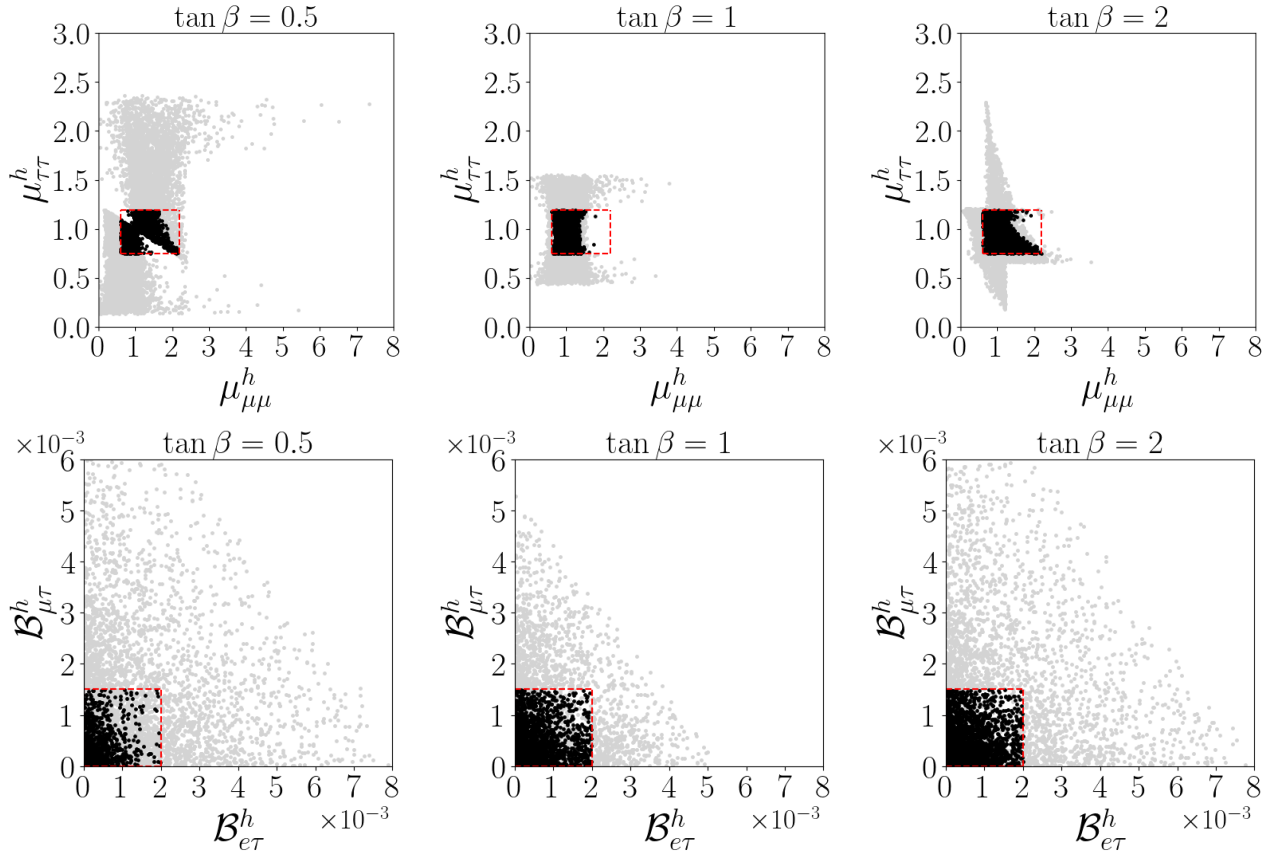


Figure 3. The impact of $\tan \beta$ on the LFC and LFV decays of h_{SM} . The color conventions are the same as in Fig. 2.

over all parameters. We see that such a scan easily produces many parameter space points that meet all six h_{SM} experimental constraints. Thus, it confirms the model's compatibility with h_{SM} leptonic decay data and allows us to continue exploration. In the subsequent discussion, we will only keep the black points, which satisfy all six leptonic decay constraints.

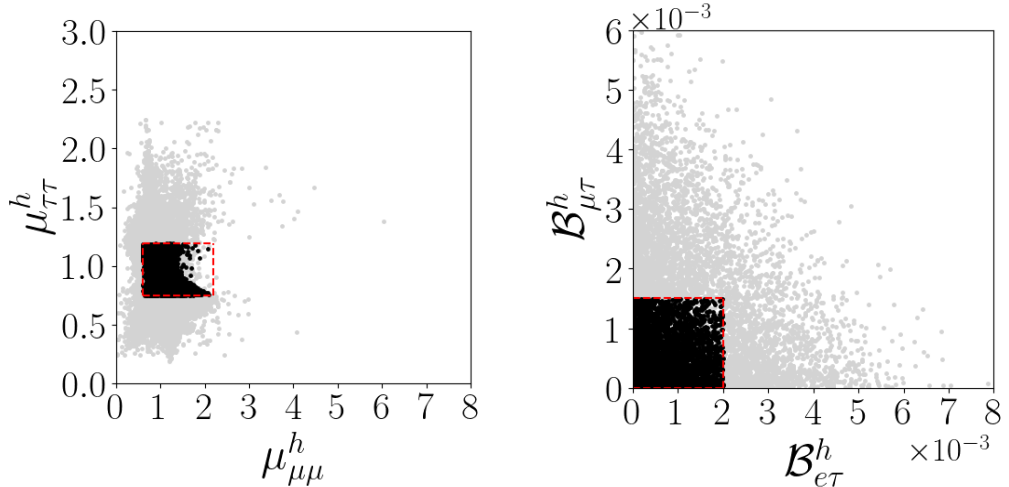


Figure 4. A comprehensive numerical scan of h_{SM} lepton decay in high-mass region.

C. Case B_1 : decay $\mu \rightarrow e\gamma$

Next, we turn to $\mu \rightarrow e\gamma$, which receives contributions from extra Higgs bosons, both neutral and charged. We first perform a numerical scan in a similar way as above: the scalar sector parameters are scanned within the ranges given in Eq. (25), while for the leptonic sector scan, we use uniform sampling of all the angles of the matrices V_L, V_R , see Appendix B for the definitions. We refer to this scan as the full Yukawa scan and show its outcome in Fig. 5.

The key observable is $\mathcal{B}_{e\gamma}^\mu \equiv \text{Br}(\mu \rightarrow e\gamma)$ shown on the horizontal axis on both plots; the vertical red dashed line indicates its MEG II upper limit 1.5×10^{-13} taken from [26]. The vertical axis on Fig. 5, left, shows one of the most constraining LFV Higgs decays, $h_{\text{SM}} \rightarrow \mu\tau$. We see that almost all points significantly exceed the MEG II upper limit, with only very few points passing this constraint.

Fig. 5, right, provides an additional insight into the dynamics of this decay. Here, we show the result of the $\mu \rightarrow e\gamma$ calculation in which only the loops with the τ lepton is taken into account. We denote the result as $\mathcal{B}_{e\gamma}^\mu(\tau)$ and show on the vertical axis of Fig. 5, right, its relative value to the full $\mathcal{B}_{e\gamma}^\mu$ calculation. The plot confirms that, for the majority of the points, the τ lepton loop dominates; moreover, the closer this ratio is to one, the easier it is to further suppress the value of $\mathcal{B}_{e\gamma}^\mu$.

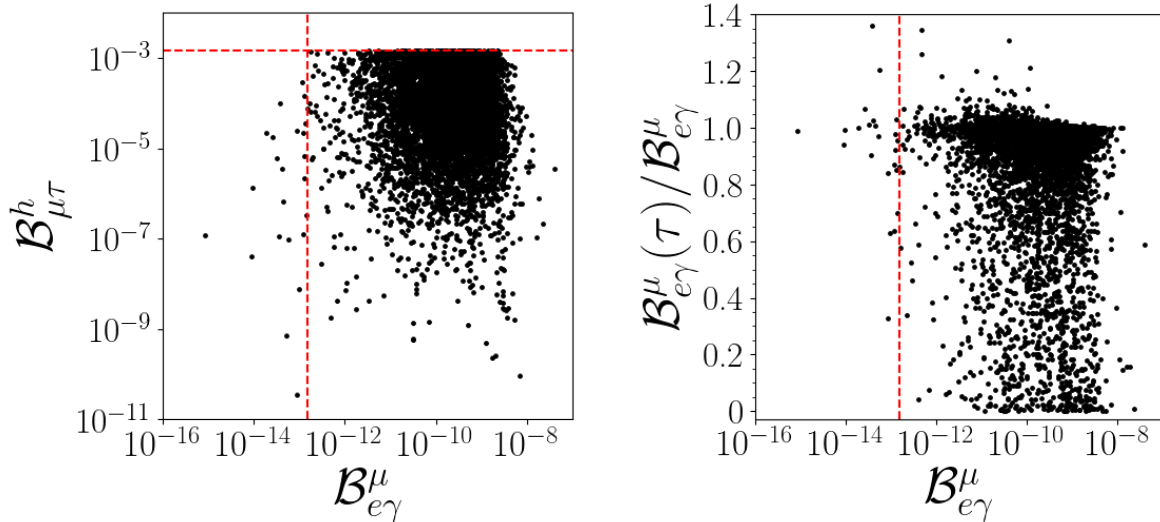


Figure 5. Left: the results of the full Yukawa scan in the plane $\mathcal{B}_{\mu\tau}^h$ vs. $\mathcal{B}_{e\gamma}^\mu$. Right: the distribution of the ratio $\mathcal{B}_{e\gamma}^\mu(\tau)/\mathcal{B}_{e\gamma}^\mu$, the contribution of τ propagator diagram to $\mu \rightarrow e\gamma$. The red dashed lines show the experimental upper limits.

This insight suggests a strategy to further suppress $\mu \rightarrow e\gamma$: we need to sample the leptonic parameter space in such a way that the LFV couplings of the τ and h_{SM} are suppressed. To this end, we follow the procedure developed in [19, 21] and perform a restricted Yukawa scan, in which we limit the angles as

$$\theta_{13}, \theta_{23} \in [-\theta_{\text{max}}, \theta_{\text{max}}], \quad \theta_{\text{max}} = \pi/100. \quad (29)$$

Then, the rotation matrices V_L and V_R of nearly block diagonal form

$$V_L, V_R \sim \begin{pmatrix} \times & \times & \cdot \\ \times & \times & \cdot \\ \cdot & \cdot & \times \end{pmatrix}, \quad (30)$$

where each \cdot stands for a non-zero but small elements, while \times denotes an element of order one. Under such approximation, N_2, N_3 simplify to

$$N_2 \sim \begin{pmatrix} \times & \cdot & \cdot \\ \cdot & \times & \cdot \\ \cdot & \cdot & \times \end{pmatrix}, \quad N_3 \sim \begin{pmatrix} \times & \times & \cdot \\ \times & \times & \cdot \\ \cdot & \cdot & \cdot \end{pmatrix}, \quad (31)$$

which automatically suppresses the contributions from the τ -induced loop to $\mathcal{B}_{e\gamma}^\mu$. Moreover, this procedure automatically suppressed the LFV Higgs boson decays $\mathcal{B}_{e\tau}^h$ and $\mathcal{B}_{\mu\tau}^h$.

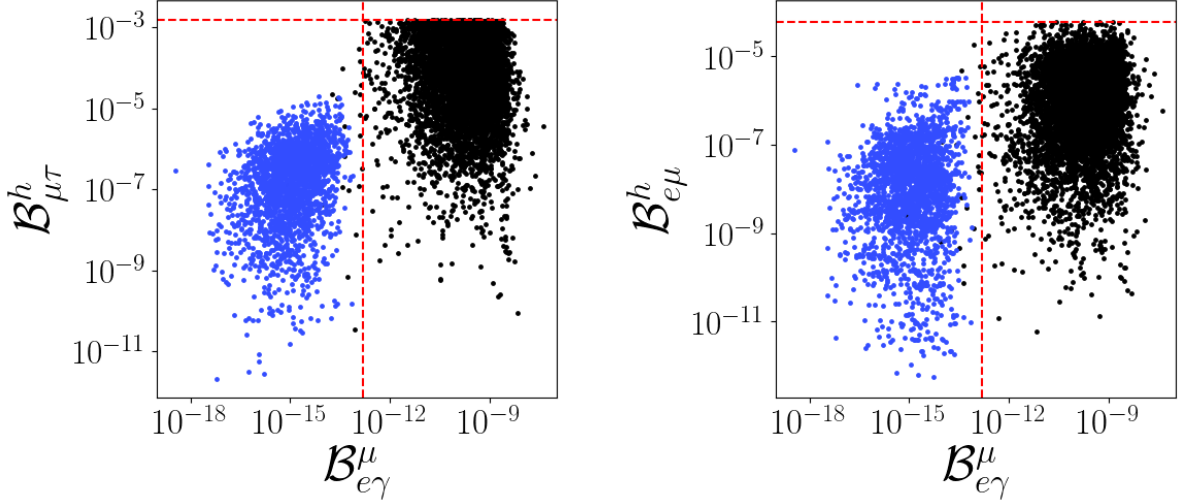


Figure 6. The distributions of $\mathcal{B}_{\mu\tau}^h$ (left plot) and $\mathcal{B}_{e\mu}^h$ (right plot) vs. $\mathcal{B}_{e\gamma}^\mu$. The black and blue points correspond to the full and restricted ($\theta_{max} = \pi/100$) Yukawa scans, respectively.

With this discussion in mind, we performed the focused Yukawa scan and compared, in Fig. 6, its outcome with the results of the full Yukawa. On both plots, the horizontal axis is again $\mathcal{B}_{e\gamma}^\mu$, while the vertical axes show two LFV Higgs boson decays. The black points correspond to the full Yukawa scan as before, while the blue points emerge from our restricted Yukawa scan. We observe a dramatic reduction in $\mathcal{B}_{e\gamma}^\mu$ and in the Higgs bosons LFV decays. With the restricted scan, almost all of the points easily pass the $\mathcal{B}_{e\gamma}^\mu$ constraints, often by several orders of magnitude.

We conclude that by implementing a restricted Yukawa scan, we can easily construct CP4-invariant leptonic cases B_1 that pass all the checks from h_{SM} leptonic decays and from $\mu \rightarrow e\gamma$.

D. Cases B_2 and B_3

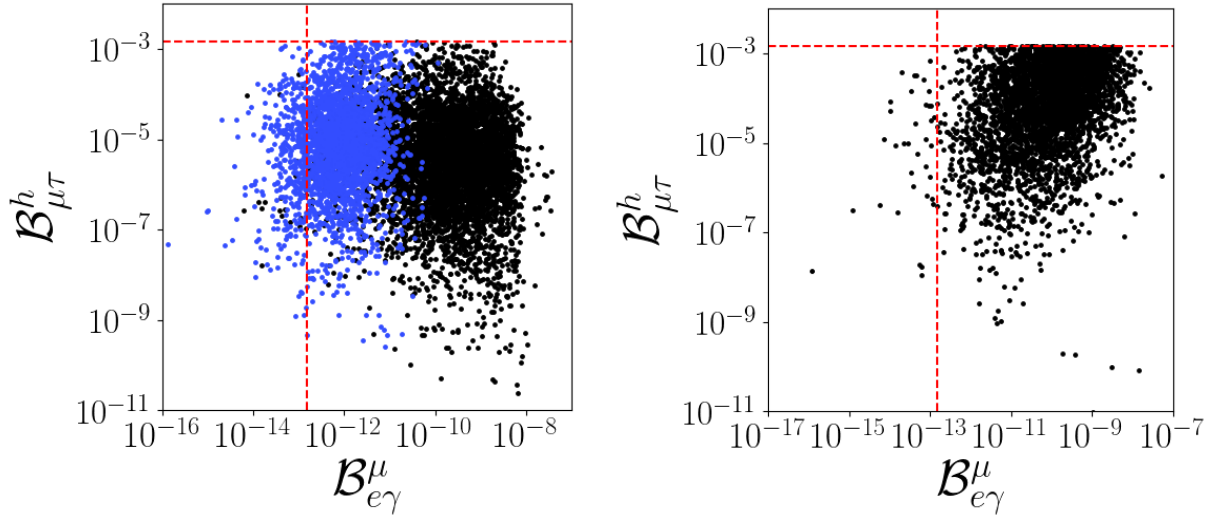


Figure 7. The full and restricted Yukawa scans for the Yukawa scenarios B_2 (left plot) and B_3 (right plot), with the same color code as in Fig. 6.

We also implemented and explored the two other CP4-invariant leptonic sectors, B_2 and B_3 . The analysis of the Higgs boson leptonic decays, both LFC and LFV, produced plots similar to Fig. 4. Although the shapes of regions covered by gray points were somewhat different, we could still find many black points that passed all six Higgs decay

constraints. However, the results on $\mathcal{B}_{e\gamma}^\mu$ shown in Fig. 7 display a very different picture than in the case B_1 . As expected, the full Yukawa scan almost always violated the $\mathcal{B}_{e\gamma}^\mu$ upper limit. However, for case B_2 , we found a different version of the restricted Yukawa scan, $\theta_{12}, \theta_{13} \in [-\theta_{max}, \theta_{max}]$, with $\theta_{max} = \pi/100$, in the right-handed lepton rotation matrix V_R . This choice led to a significant reduction of the $\mathcal{B}_{e\gamma}^\mu$ decay rate. The results of this scan are shown by blue points in Fig. 7, left. Still, for most of the points, the suppression is insufficient. Although this scenario is not readily excluded, it appears very fine-tuned, with little margin remaining. In the light of further uncertainties in computation of $\mathcal{B}_{e\gamma}^\mu$, including the two-loop contributions which are still debated, we do not consider this scenario promising.

As for the scenario B_3 , the special form of its Yukawa coupling patterns discussed in [19] does not allow for any simple restriction on the rotation matrix angles that could help us significantly suppress $\mathcal{B}_{e\gamma}^\mu$. We consider this case to be nearly ruled out by the MEG II upper limit.

In short, we believe that case B_1 is the most promising candidate for a non-trivial extension of the CP4 symmetry to the leptonic sector.

IV. NEW LEPTONIC SIGNATURES FROM ADDITIONAL HIGGS BOSONS

The previous section dealt with the leptonic decays of the SM-like Higgs boson as well as the $\mu \rightarrow e\gamma$ decays. However, the multi-Higgs model we consider contains many more Higgs scalars, which can also couple to leptons and lead to leptonic signals at different invariant masses. In the vicinity of the alignment limit, it is natural to expect that all these potential signals are suppressed. In fact, for $\epsilon = 0$, such signals vanish altogether, at least at tree level.

However, it turns out that the LHC data actually do contain hints of new scalars decaying leptonically. Indeed, the CMS collaboration reported in [44] an intriguing $e\mu$ excess for a new resonance at the invariant mass of 146 GeV, with a local significance of 3.8σ and a global significance of 2.8σ . Such a signal could be accommodated in many models, including ours. However, most models predict that an $H \rightarrow e\mu$ hint should be accompanied by other leptonic signals at the same invariant mass, both LFC and LFV. The exact relation among these signals depends on the model and on the values of its free parameters. In particular, CP4 3HDM may lead to peculiar results, just because the CP4 symmetry necessarily involves generation mixing transformations and, as a result, the leptonic coupling matrices Y_{ij}^k in Eq. (19) do not necessarily follow the traditional generation hierarchy as typically found in the 2HDM. Thus, it is an interesting question whether the predictions of the other channels are compatible with non-observation of a corresponding signal.

This is what we report in this section. We consider the CP4 3HDM points with the Yukawa scenario B_1 that pass all the constraints discussed previously and select only those of them that contain a new neutral Higgs boson, denoted as h_{146} , in the mass range 140–150 GeV, the exact value 146 GeV being inessential in our study. To get a broad picture without unnecessary complications, we also require that h_{146} is the only new Higgs boson in this mass range.

Next, since we do not know the preferred production and decay channels for h_{146} , we cannot separately predict its production cross section and its decay preferences. However, we do not need that information. We simply rely on the CMS central value for $\sigma(pp \rightarrow h_{146} \rightarrow e\mu) = 3 \text{ fb}$ and define the other leptonic signals as

$$\sigma(pp \rightarrow h_{146} \rightarrow \ell_i \ell_j) = \sigma(pp \rightarrow h_{146} \rightarrow e\mu) \times \frac{\Gamma(h_{146} \rightarrow \ell_i \ell_j)}{\Gamma(h_{146} \rightarrow e\mu)}. \quad (32)$$

Although the direct experimental upper limits for the h_{146} signal in various $\ell_i \ell_j$ channels are not available, the ATLAS and CMS collaborations published the results of their generic new scalar searches in various leptonic final states [45–48, 52]. We studied the data point distributions in the invariant mass range of interest, compared them with the h_{SM} signal (if detected) and upper limits (if not seen), and knowing the SM-Higgs production cross section, we conservatively placed the following constraints:

$$\begin{aligned} \sigma(pp \rightarrow h_{146} \rightarrow ee) &< 10 \text{ fb}, & \sigma(pp \rightarrow h_{146} \rightarrow \mu\mu) &< 4 \text{ fb}, & \sigma(pp \rightarrow h_{146} \rightarrow \tau\tau) &< 1000 \text{ fb}, \\ \sigma(pp \rightarrow h_{146} \rightarrow e\tau) &< 100 \text{ fb}, & \sigma(pp \rightarrow h_{146} \rightarrow \mu\tau) &< 100 \text{ fb}. \end{aligned} \quad (33)$$

In Fig. 8, we illustrate the results of this study with a representative plot of $\sigma(pp \rightarrow h_{146} \rightarrow \mu\mu)$ vs. $\sigma(pp \rightarrow h_{146} \rightarrow ee)$. We stress again that all points already satisfy the constraints discussed in the previous section. Among them, black points correspond to the cases when all $\sigma(pp \rightarrow h_{146} \rightarrow \ell_i \ell_j)$ signals satisfy the experimental limits in Eq. (33). The most salient feature of this plot is the sheer range of the values that $\sigma(pp \rightarrow h_{146} \rightarrow \mu\mu)$ and $\sigma(pp \rightarrow h_{146} \rightarrow ee)$ can attain even when $\sigma(pp \rightarrow h_{146} \rightarrow e\mu)$ is fixed at 3 fb, which highlights the peculiar couplings of a new Higgs boson across leptonic generations. Many of the points are excluded by orders of magnitude, but there also remain many examples where the signals are well below the current upper limits. Note also that the ee channel is not always suppressed—let alone suppressed by $(m_e/m_\mu)^2$ —with respect to the $\mu\mu$ channel. In fact, typical are the situations

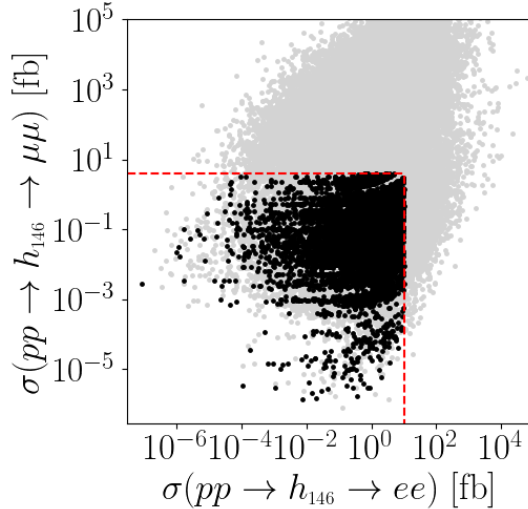


Figure 8. The distribution of the leptonic signals $\sigma(pp \rightarrow h_{146} \rightarrow ee)$ and $\sigma(pp \rightarrow h_{146} \rightarrow \mu\mu)$ in the CP4 3HDM with scenario B_1 passing all the h_{SM} and $\mu \rightarrow e\gamma$ constraints. The points that satisfy all six new experimental limits for h_{146} are shown by black dots.

where the ee channel dominates over $\mu\mu$ and $e\mu$. All these features are the echo of the peculiar form of the CP4 symmetry of the original lagrangian.

This finding has interesting implications for future experimental searches. The current collider searches of the additional Higgs bosons via leptonic channels focus on LFV channels like $e\mu$. However, our results show that the ee decay channel of h_{146} could also be within the reach of the HL-LHC [53] and at the future e^+e^- factories; in any case, the new experimental data, even if the search results are negative, will further exclude significant parts of these points.

Thus, the tentative 146 GeV Higgs boson signal seen by CMS can be interpreted within CP4 3HDM case B_1 and leads to experimentally testable predictions. Its characteristic leptonic decay signatures, with the ee , $\mu\mu$, $e\mu$ rates being of the same order of magnitude, offers a distinct experimental method that sets it apart from conventional Higgs scenarios, such as the 2HDM. Future collider BSM Higgs program should definitely include the ee decay channel, an underappreciated probe at present.

V. SUMMARY

In summary, the CP4 3HDM, a unique three-Higgs-doublet model with an exact CP symmetry of order 4, exhibits peculiar scalar and Yukawa sector properties that have been addressed in several studies. However, its impact on the lepton sector and lepton-scalar couplings has never been evaluated. This is what we did in the present work. We compared the lepton flavor conserving and violating decays of the 125 GeV Higgs boson h_{SM} and the LFV decay $\mu \rightarrow e\gamma$ with experimental constraints. Relying in the insights into the structure of the scalar and Yukawa sectors of the model presented in the recent papers [18, 21], we set up an efficient scanning procedure and indeed found, in the scenario B_1 , well-defined parameter space regions where the predictions are well within experimental limits, with a large margin. In contrast, the other two CP4 scenarios, B_2 and B_3 typically lead to much larger $\mu \rightarrow e\gamma$ rates and are nearly excluded.

Now, after [21] and the present work, there emerges an interesting conclusion: the only CP4-invariant Yukawa sectors that are safely compatible with flavor and lepton observables are B_1 for the leptonic sector, A for the down-quark sector, and B_2 for the up-quark sector. It is at present unclear whether this observation is indicative of any structural feature of the model.

We conclude by stating that CP4 3HDM, with its peculiar symmetry and phenomenology, is still consistent with experimental data, at least in those scalar, quark, and lepton channels that have been considered so far. Curiously, out of many CP4-invariant Yukawa sectors, only one is not excluded and is well within the limits. Moreover, it leads to interesting predictions, such as the potentially large $h_{146} \rightarrow ee$ signal. However, we have not yet included the full body of experimental results available today. Thus, it remains an intriguing question whether this unique version of the three-Higgs-doublet model is indeed compatible with all searches and signals we have at present, or whether it

will eventually be ruled out by any specific measurement not included in this work. The fate of CP4 3HDM remains to be settled.

ACKNOWLEDGMENTS

This work was supported by Guangdong Natural Science Foundation (project No. 2024A1515012789).

Appendix A: Yukawa coupling matrices N_2 and N_3

For the sake of completeness, we outline here the expression for the Yukawa coupling matrices N_2 and N_3 for all three non-trivial CP4 leptonic sectors. These expressions coincide with the down-quark sector matrices derived in [19], with the obvious replacement of the masses and rotation matrices.

In case B_1 , the expression for N_2^0 in Eq. (12) can be written as

$$N_2^0 = M_e^0 \cot \beta - \frac{v}{\sqrt{2} s_\beta} \Gamma_1 = R_3^0 \cdot M_e^0. \quad R_3^0 = \text{diag}(\cot \beta, \cot \beta, -\tan \beta). \quad (\text{A1})$$

After the mass matrix diagonalization, we obtain $N_2 = V_L^\dagger R_3^0 V_L \cdot M_e$. As for N_3^0 , we can present it as

$$N_3^0 = \frac{1}{s_\beta} P_4 \cdot M_d^{0*} \cdot R_2, \quad \text{where} \quad P_4 = \begin{pmatrix} 0 & -1 & 0 \\ 1 & 0 & 0 \\ 0 & 0 & 0 \end{pmatrix}, \quad R_2 = \begin{pmatrix} 0 & 1 & 0 \\ 1 & 0 & 0 \\ 0 & 0 & 1 \end{pmatrix}. \quad (\text{A2})$$

After the lepton field rotations, we get

$$N_3 = \frac{1}{s_\beta} V_L^\dagger P_4 V_L^* \cdot M_e \cdot V_R^T R_2 V_R, \quad (\text{A3})$$

For case B_2 , following the same logic, we write

$$N_2 = M_d \cdot V_R^\dagger R_3^0 V_R, \quad (\text{A4})$$

$$N_3 = \frac{1}{s_\beta} V_L^\dagger R_2 V_L^* \cdot M_e \cdot V_R^T P_4 V_R. \quad (\text{A5})$$

Finally, for case B_3 , the expressions are

$$N_2 = M_d \cot \beta - \frac{1}{s_\beta c_\beta} \left(V_L^\dagger P_3 V_L^* \cdot M_e \cdot V_R^T P_3 V_R - V_L^\dagger P_4 V_L^* \cdot M_e \cdot V_R^T P_4 V_R \right), \quad (\text{A6})$$

$$N_3 = \frac{1}{s_\beta} \left(V_L^\dagger P_4 V_L^* \cdot M_e \cdot V_R^T P_3 V_R + V_L^\dagger P_3 V_L^* \cdot M_e \cdot V_R^T P_4 V_R \right). \quad (\text{A7})$$

where $P_3 = \text{diag}(0, 0, 1)$.

Appendix B: A general $U(3)$ rotation matrix

We construct $U(3)$ rotation matrices V_L and V_R using the Chau-Keung form:

$$V = \begin{pmatrix} e^{i\psi_1} & 0 & 0 \\ 0 & e^{i\psi_2} & 0 \\ 0 & 0 & e^{i\psi_3} \end{pmatrix} \begin{pmatrix} 1 & 0 & 0 \\ 0 & c_{23} & s_{23} \\ 0 & -s_{23} & c_{23} \end{pmatrix} \begin{pmatrix} c_{13} & 0 & s_{13} e^{-i\delta} \\ 0 & 1 & 0 \\ -s_{13} e^{i\delta} & 0 & c_{13} \end{pmatrix} \begin{pmatrix} c_{12} & s_{12} & 0 \\ -s_{12} & c_{12} & 0 \\ 0 & 0 & 1 \end{pmatrix} \begin{pmatrix} e^{i\varphi_1} & 0 & 0 \\ 0 & e^{i\varphi_2} & 0 \\ 0 & 0 & e^{i\varphi_3} \end{pmatrix}. \quad (\text{B1})$$

Here, we use shorthand notation $s_{ij} \equiv \sin \theta_{ij}$, $c_{ij} \equiv \cos \theta_{ij}$. Since the simultaneous shift of all ψ_i and all φ_i does not change the result, we set $\varphi_3 = 0$.

[1] T. D. Lee, Phys. Rev. D **8**, 1226-1239 (1973).

- [2] S. Weinberg, Phys. Rev. Lett. **37**, 657 (1976).
- [3] G. C. Branco, P. M. Ferreira, L. Lavoura, M. N. Rebelo, M. Sher and J. P. Silva, Phys. Rept. **516**, 1-102 (2012).
- [4] I. P. Ivanov, Prog. Part. Nucl. Phys. **95**, 160-208 (2017).
- [5] I. P. Ivanov, V. Keus and E. Vdovin, J. Phys. A **45**, 215201 (2012).
- [6] I. P. Ivanov and E. Vdovin, Eur. Phys. J. C **73**, no.2, 2309 (2013).
- [7] I. P. Ivanov and C. C. Nishi, JHEP **01**, 021 (2015).
- [8] N. Darvishi and A. Pilaftsis, Phys. Rev. D **101**, no.9, 095008 (2020).
- [9] A. Kunčinas, P. Osland and M. N. Rebelo, [arXiv:2512.07657 [hep-ph]].
- [10] I. P. Ivanov and J. P. Silva, Phys. Rev. D **93**, no.9, 095014 (2016).
- [11] G. Ecker, W. Grimus and H. Neufeld, J. Phys. A **20**, L807 (1987).
- [12] W. Grimus and M. N. Rebelo, Phys. Rept. **281**, 239-308 (1997).
- [13] G. C. Branco, L. Lavoura and J. P. Silva, “CP Violation,” Int. Ser. Monogr. Phys. **103**, 1-536 (1999).
- [14] M. Maniatis, A. von Manteuffel and O. Nachtmann, Eur. Phys. J. C **57**, 739-762 (2008).
- [15] P. M. Ferreira, H. E. Haber and J. P. Silva, Phys. Rev. D **79**, 116004 (2009).
- [16] M. Maniatis and O. Nachtmann, JHEP **05**, 028 (2009).
- [17] P. M. Ferreira, I. P. Ivanov, E. Jiménez, R. Pasechnik and H. Serôdio, JHEP **01**, 065 (2018).
- [18] B. Liu, I. P. Ivanov and J. Gonçalves, JHEP **02**, 069 (2025).
- [19] D. Zhao, I. P. Ivanov, R. Pasechnik and P. Zhang, JHEP **04**, 116 (2023).
- [20] I. P. Ivanov and S. A. Obodenko, Universe **7**, no.6, 197 (2021).
- [21] D. Zhao and I. P. Ivanov, Phys. Rev. D **112**, no.9, 9 (2025).
- [22] R. H. Bernstein and P. S. Cooper, Phys. Rept. **532**, 27-64 (2013).
- [23] M. Lindner, M. Platscher and F. S. Queiroz, Phys. Rept. **731**, 1-82 (2018).
- [24] M. Ardu and G. Pezzullo, Universe **8**, no.6, 299 (2022).
- [25] A. K. Perrevoort [Mu3e], PoS **FPCP2023**, 015 (2023).
- [26] K. Afanaciev *et al.* [MEG II], Eur. Phys. J. C **85**, no.10, 1177 (2025) [erratum: Eur. Phys. J. C **85**, no.11, 1317 (2025)].
- [27] M. Aoki *et al.* [COMET, MEG, Mu2e and Mu3e], [arXiv:2503.22461 [hep-ex]].
- [28] S. Navas *et al.* [Particle Data Group], Phys. Rev. D **110**, no.3, 030001 (2024).
- [29] G. Feinberg and S. Weinberg, Nuovo Cimento **14**, 571 (1959).
- [30] T. D. Lee and G. C. Wick, Phys. Rev. **148**, 1385-1404 (1966).
- [31] S. Weinberg, “The Quantum theory of fields. Vol. 1: Foundations”, Cambridge University Press (1995).
- [32] R. González Felipe, I. P. Ivanov, C. C. Nishi, H. Serôdio and J. P. Silva, Eur. Phys. J. C **74**, no.7, 2953 (2014).
- [33] I. P. Ivanov, JHEP **02**, 025 (2018).
- [34] F. P. An *et al.* [Daya Bay], Phys. Rev. Lett. **133**, no.15, 151801 (2024).
- [35] S. Aiello *et al.* [KM3NeT], JHEP **10**, 206 (2024).
- [36] K. Abe *et al.* [Super-Kamiokande], Phys. Rev. D **109**, no.9, 092001 (2024).
- [37] T. Wester *et al.* [Super-Kamiokande], Phys. Rev. D **109**, no.7, 072014 (2024).
- [38] S. Weinberg, Phys. Rev. Lett. **63**, 2333 (1989).
- [39] S. M. Barr and A. Zee, Phys. Rev. Lett. **65**, 21-24 (1990) [erratum: Phys. Rev. Lett. **65**, 2920 (1990)].
- [40] D. A. Dicus, Phys. Rev. D **41**, 999 (1990).
- [41] A. Crivellin, A. Kokulu and C. Greub, Phys. Rev. D **87**, no.9, 094031 (2013).
- [42] M. P. Bento, J. C. Romão and J. P. Silva, JHEP **08**, 273 (2022).
- [43] W. Grimus, L. Lavoura, O. M. Ogreid and P. Osland, Nucl. Phys. B **801**, 81-96 (2008).
- [44] A. Hayrapetyan *et al.* [CMS], Phys. Rev. D **108**, no.7, 072004 (2023).
- [45] G. Aad *et al.* [ATLAS], JHEP **07**, 166 (2023).
- [46] A. M. Sirunyan *et al.* [CMS], Phys. Rev. D **104**, no.3, 032013 (2021).
- [47] A. Tumasyan *et al.* [CMS], Phys. Lett. B **846**, 137783 (2023).
- [48] G. Aad *et al.* [ATLAS], Phys. Rev. Lett. **135**, no.23, 231802 (2025).
- [49] G. Aad *et al.* [ATLAS], Nature **607**, no.7917, 52-59 (2022) [erratum: Nature **612**, no.7941, E24 (2022)].
- [50] A. Tumasyan *et al.* [CMS], Nature **607**, no.7917, 60-68 (2022) [erratum: Nature **623**, no.7985, E4 (2023)].
- [51] D. de Florian *et al.* [LHC Higgs Cross Section Working Group], CERN Yellow Rep. Monogr. **2**, 1-869 (2017).
- [52] A. Tumasyan *et al.* [CMS], Eur. Phys. J. C **83** (2023) no.7, 562
- [53] M. Cepeda, S. Gori, P. Ilten, M. Kado, F. Riva, R. Abdul Khalek, A. Aboubrahim, J. Alimena, S. Alioli and A. Alves, *et al.* CERN Yellow Rep. Monogr. **7** (2019), 221-584.